ELSEVIER

International Journal of Solids and Structures 41 (2004) 1991–2009

INTERNATIONAL JOURNAL OF SOLIDS and STRUCTURES

www.elsevier.com/locate/ijsolstr

FEM formulation of four and five noded elements using a linearly varying stress assumption

John F. Peters [a], Ernest Heymsfield [b,*]

[a] *USAE Waterways Experiment Station, Vicksburg, MS, 39180, USA*

[b] *Department of Civil Engineering, University of Arkansas, 4160 Bell Engineering Center, Fayetteville, AR 72701, USA*

Received 12 February 2003; received in revised form 29 October 2003

Abstract

The two-dimensional stress analysis is investigated to develop multi-noded elements that can be used in a finite element mesh. To accomplish this, a hybrid stress element is developed assuming a linear stress variation within the element. The formulation for this type of element is developed for a multi-noded polygon consisting of up to five nodes however simplifies to a constant stress element for a triangle. The formulation differs from the method developed by Pian [AIAA J. 2 (1964) 1333]. In the formulation discussed in this article, the same matrix is used to relate stress to constant stress parameters, and strain to constant strain parameters. This approximation simplifies the formulation, however does not significantly impact the results. The effectiveness of the formulation and code implementation is illustrated through ''patch tests'' along with other examples to assess this approximation. The linear stress element developed in this article is shown to be robust, yielding reasonable results even when a poorly designed finite element mesh is used in the cantilever beam example. In addition, the article includes a comparison between the linear stress element and the constant strain element to illustrate the advantages of the linear stress element over the constant strain element approach.

Keywords: Hybrid stress element; Linear stress element; Finite elements

1. Introduction

The unstructured character of finite element meshes makes the finite element method well suited for problems involving complex boundary geometry and material heterogeneity. The finite element method has been found especially appropriate for soil–structure interaction problems. In problems involving complex geometries or material heterogeneity, combinations of triangular and quadrilateral elements are typically used. However, when there is excessive use of triangular elements, to accommodate a complex geometry or when poorly shaped elements are used, numerical problems develop. To avoid excessive stiffness due to the overuse of triangular elements, a mesh should be configured to primarily employ quadrilateral elements and

* Corresponding author. Tel.: +1-479-575-7586; fax: +1-479-575-7168.

E-mail addresses: petersj@wes.army.mil (J.F. Peters), ernie@uark.edu (E. Heymsfield).

0020-7683/$ - see front matter © 2003 Elsevier Ltd. All rights reserved.
doi:10.1016/j.ijsolstr.2003.11.019

limit the use of triangular or other multi-noded elements, to areas where transition elements are warranted. Five noded elements are beneficial to use in these transition areas. In the article by Peters and Heymsfield, the use of elements comprised of an arbitrary number of nodes was investigated using the constant strain assumption (Peters and Heymsfield, 2003). Although the constant strain element was found to be robust, the element is dependent on a stabilization parameter to prevent zero energy spurious mode shapes, "hourglassing", from developing. However, the specific value of the stabilization parameter was found to be definite only for rectangular elements. For other polygon elements, the stabilization parameter is indefinite and is normally chosen to be an arbitrarily large number to control bending.

The issue of stabilization is central to development of an efficient finite element. Full integration of two-dimensional quadrilateral finite elements generally uses two-point quadrature in which integration is made using four integration points. Fully integrated elements are expensive and have poor convergence properties for nearly incompressible materials. To both reduce computation time and improve convergence, one-point quadrature is commonly used. However, characteristic of the one-point quadrature approach is the instability that develops in elements of four or more nodes. An extensive body of literature now exists on the stabilization problem, a summary of which is included in the paper by Peters and Heymsfield (2003).

This paper investigates an alternative approach to the constant strain approach. The approach discussed in this paper is applicable to polygons consisting of either four or five nodes and remedies the problem of stabilization that is intrinsic to the constant strain approach. The proposed method obviates the need of a stabilization factor by assuming a stress distribution within the element. The approach is similar to the hybrid stress element developed by Pian (1964), however differs in that the formulation discussed in this paper is established through energy balance and arrives at consistent multipliers for stress and strain constants via the virtual work principle rather than invoking Lagrange multipliers.

Three approaches appear in literature to develop suitable elements to use for coarse meshes with significant bending behavior. These approaches include assuming a stress field within the element, assuming a strain field, or a combination of an assumed stress and strain field. An example of an assumed strain field approach is found in the reference by Simo and Rifai (1990). Their approach uses the method of incompatible modes to develop three different types of elements including a plane elastic quad, an axisymmetric element, and a thick plate bending quadrilateral. In the element formulation, Simo and Rifai supplement the symmetric gradient of the displacement field with an enhanced strain field to arrive at a total strain field within the element. The benefit of their approach includes the elimination of the stress field from the element formulation by orthogonality of the stress field to the enhanced strain field. The previous cited work by Simo and Rifai was extended to nonlinear elastic and finite strain plasticity problems in the companion reference by Simo and Armero (1992). In this second reference on nonlinear problems, the displacement gradient is developed by supplementing the actual displacement gradient by an enhanced displacement gradient.

Initial work for an element assuming a stress field was made by Pian (1964). In the formulation, the stress field within the element is written as a function of five undetermined stress coefficients, which are constants, and the element coordinate system. Selection of the stress distribution is based on satisfying equations of equilibrium within the element. Through minimizing the total complementary energy of the element, the particular stress coefficients can be determined. Tong and Pian extended Pian's prior work by including element body forces and showing Pian's derivation to be the employment of a variational principle (Tong and Pian, 1969). As a result, a functional related to the assumed stress element was able to be determined. Convergence was investigated in the Tong and Pian study and found to be dependent on improving both stress and displacement approximations concurrently. Wolf (1975) developed an alternative model to the Pian hybrid stress element. In the Wolf model, an equation for stress expansion is established, so that stress equilibrium is satisfied on an average sense within the element, yet force equilibrium is satisfied along all points on the inter-element boundary. This approach was found to be especially suitable for shell type problems. Suitability of the Wolf formulation was shown by using triangular elements for thick

plate problems and for doubly curved shallow thin shell problems (Wolf, 1975). Additional improvements to the hybrid stress element were made using the Hellinger-Reissner principle (Pian and Sumihara, 1984) and revising the formulation by initially assuming decoupled stresses. In addition, constraints were applied in a variational sense through internal displacements. The benefits of implementing such an approach allows a rational basis to obtain assumed stress distributions within geometrically distorted elements. A recent article by Pian summarizes the early development of the hybrid stress element (Pian, 2000).

A combination of an assumed stress and strain field is found in the work by Piltner and Taylor (1995). In the reference, Piltner and Taylor develop a plane strain/stress element, QE2, by using incompatible displacements in addition to compatible displacements. The element is developed using a modified Hu-Washizu variational formulation where the modification is made by including an enhanced strain field term. Seven stress and strain terms are used in Cartesian co-ordinates. An optimal number of parameters to describe the element is five. Therefore, to improve element performance, the element is made more flexible by including two enhanced strain modes. In comparison with the work by Simo and Rifai (1990), Piltner and Taylor set the reference stresses, constant stress and linear stress terms, rather than the total stress field, orthogonal to the enhanced strain field. An alternative formulation to the QE2 element is discussed in a later paper by Piltner and Taylor (1999). In this latter paper, the QE2 formulation is modified to improve numerical computation by using B-bar functions. The B-bar functions were found to simplify matrix computations without compromising numerical accuracy.

The element formulation described in this paper assumes a stress field within the element. The element is especially attractive because its computational cost is comparable to one-point Gaussian quadrature and is easy to implement. The element is similar to that used for the hybrid stress element however differs in details. The element used in this formulation represents a polygonal-shaped sub-domain within which the stress varies linearly. Therefore, the formulation is generalized to be applicable to a polygonal element with a maximum of five nodes. A consequence of the linear stress distribution assumption within the element is that stresses vary linearly along the element boundary. Although the assumed linear stress distribution does not result in a linear displacement field along the element boundary, displacements are assumed to vary linearly between nodes for element compatibility (Gallagher, 1965). Even with the ostensible incompatibility, reliable results are attained. Several example problems are considered in this study to show the suitability of the formulation.

This paper consists of three parts. The first part describes the element formulation. In the second part, the validity of the approach is demonstrated through patch tests. Included in the patch tests is the applicability of the approach to a mesh consisting of elements with four and five nodes. The third part presents examples of the element's performance.

2. Linear stress element formulation

The linear stress formulation in this article is developed through virtual work and is therefore not limited to linear elastic behavior. The work balance for a virtual deformation is given by

$$\{f\}^{\mathrm{T}}\{a\} = \int_{V^{\mathrm{e}}} \{\sigma\}^{\mathrm{T}}\{\varepsilon\}\,\mathrm{d}V \tag{1}$$

where f represents work-equivalent loads acting on the element at the nodal points. The product of these work-equivalent loads, f, and node displacements, a, represents the work of the surface tractions along the element boundary.

For this particular formulation, a linear stress distribution is assumed to occur within the element. The stresses in the element are written in terms of the stress at the centroid of the element and constant multipliers to include for the gradient of the stress within the element:

$$\begin{Bmatrix} \sigma_{xx} \\ \sigma_{yy} \\ \sigma_{xy} \end{Bmatrix} = \begin{Bmatrix} \sigma^0_{xx} + ax + by \\ \sigma^0_{yy} + cx + dy \\ \sigma^0_{xy} + ex + fy \end{Bmatrix} \tag{2}$$

Eq. (2) is a function of nine constants. Eq. (2) can be reduced by relating constants e and f, to a and d using the stress equilibrium equations. By applying these equilibrium equations, Eq. (2) is reduced to seven constants:

$$\begin{Bmatrix} \sigma_{xx} \\ \sigma_{yy} \\ \sigma_{xy} \end{Bmatrix} = \begin{Bmatrix} \sigma^0_{xx} + ax + by \\ \sigma^0_{yy} + cx + dy \\ \sigma^0_{xy} - dx - ay \end{Bmatrix} \tag{3}$$

Eq. (3) is now rewritten in terms of a matrix, H, and a vector, σ^*, which includes the constant stress parameters:

$$\{\sigma\} = [H]\{\sigma^*\} \tag{4}$$

where

$$[H] = \begin{bmatrix} 1 & 0 & 0 & x & y & 0 & 0 \\ 0 & 1 & 0 & 0 & 0 & x & y \\ 0 & 0 & 1 & -y & 0 & 0 & -x \end{bmatrix} \tag{5}$$

and

$$\{\sigma^*\} = \begin{Bmatrix} \sigma^0_{xx} & \sigma^0_{yy} & \sigma^0_{xy} & a & b & c & d \end{Bmatrix}^{\mathrm{T}} \tag{6}$$

The same matrix, H, used to relate stress within the element to the constant stress parameters in Eq. (4) is used to approximately relate strain within the element to the constant strain parameters:

$$\{\varepsilon\} = [H]\{\varepsilon^*\} \tag{7}$$

where

$$\{\varepsilon\} = \begin{Bmatrix} \varepsilon_{xx} & \varepsilon_{yy} & \varepsilon_{xy} \end{Bmatrix}^{\mathrm{T}} \tag{8}$$

and

$$\{\varepsilon^*\} = \begin{Bmatrix} \varepsilon^0_{xx} & \varepsilon^0_{yy} & \varepsilon^0_{xy} & k & l & m & n \end{Bmatrix}^{\mathrm{T}} \tag{9}$$

This approximation leads to the same matrix being used to relate the constant stress parameters with nodal forces, and nodal displacements with the constant strain parameters. The strain expression in Eq. (9) is a function of seven constants. Therefore, the strain will not necessarily satisfy the constitutive relationship throughout the element, but instead on an approximate basis. Therefore, element strains are not satisfied on a point-to-point basis however satisfy the work consistent definition of strain.

To derive the element stiffness matrix, Eq. (1) is used to solve for f in the form of $[K]\{a\}$ where K is a function of element geometry, stress parameters (σ^*), and strain parameters (ε^*). Eqs. (4) and (7) are substituted into the right hand side of Eq. (1) to determine the internal work, W^{i}, of the element in terms of the constant stress and strain parameters:

$$W^{\mathrm{i}} = \{\sigma^*\}^{\mathrm{T}}[\lambda]\{\varepsilon^*\} \tag{10}$$

where

$$[\lambda] = \int_{V^{\mathrm{e}}} [H]^{\mathrm{T}}[H]\,\mathrm{d}V \tag{11}$$

In Eq. (11), λ is symmetric and is a function only of the geometry of the element. Therefore, by using the same matrix to relate stress to stress parameters and strain to strain parameters, λ becomes symmetric. Taking the origin of the element coordinate system at the element centroid, λ simplifies to

$$[\lambda] = \begin{bmatrix} [V^e] & 0 & 0 & 0 & 0 \\ 0 & I_{xx}+I_{yy} & I_{xy} & 0 & I_{xy} \\ 0 & I_{xy} & I_{xx} & 0 & 0 \\ 0 & 0 & 0 & I_{yy} & I_{xy} \\ 0 & I_{xy} & 0 & I_{xy} & I_{xx}+I_{yy} \end{bmatrix} \tag{12}$$

where I_{xx} and I_{yy} are the moments of inertia about the x and y axes respectively. I_{xy} is the product of inertia and V^e is a diagonal matrix with the element area as entries:

$$[V^e] = \begin{bmatrix} V^e & 0 & 0 \\ 0 & V^e & 0 \\ 0 & 0 & V^e \end{bmatrix} \tag{13}$$

The external work of the nodal forces, W^e, on the element is similarly written in terms of the constant stress parameters, σ^*. To relate the constant stress parameters to work-equivalent loads, surface tractions are written in terms of the constant stress parameters, and a nodal force–stress matrix, $[S]$:

$$\{f\} = [S]\{\sigma^*\} \tag{14}$$

The S matrix is developed by writing the stress resultants along the element boundary in terms of the seven stress parameters in Eq. (6) and the normal to the boundary. A linearly varying displacement field is assumed along the element boundary. Therefore the contribution to the nodal force at node i from element $i-j$ in the k direction, $f_{i-ij,k}$, is

$$f_{i-ij,k} = \frac{t_{i,k}L_{ij}}{3} + \frac{t_{j,k}L_{ij}}{6} \tag{15}$$

and to the nodal force at node j, $f_{j-ij,k}$:

$$f_{j-ij,k} = \frac{t_{i,k}L_{ij}}{6} + \frac{t_{j,k}L_{ij}}{3} \tag{16}$$

$t_{i,k}$ and $t_{j,k}$ are the stress resultants in the k direction at nodes i and j respectively. L_{ij} is the element boundary length between nodes i and j. The stress resultants at node i are a function of the boundary normal and related to stresses at node i by

$$t_{i,k} = \sigma_{km} n_m \tag{17}$$

Indicial notation is used in Eq. (17) and n_m is the normal component in the m direction. Eq. (4) is used to write Eqs. (15) and (16) in terms of the stress parameters of Eq. (6). For an element of n nodes, the nodal force–stress matrix, S, is

$$[S] = \begin{bmatrix} C_{11} & 0 & C_{13} & C_{14} & C_{15} & 0 & C_{17} \\ 0 & C_{13} & C_{11} & -C_{15} & 0 & -C_{17} & -C_{14} \\ C_{21} & 0 & C_{23} & C_{24} & C_{25} & 0 & C_{27} \\ 0 & C_{23} & C_{21} & -C_{25} & 0 & -C_{27} & -C_{24} \\ \vdots & \vdots & \vdots & \vdots & \vdots & \vdots & \vdots \\ C_{n1} & 0 & C_{n3} & C_{n4} & C_{n5} & 0 & C_{n7} \\ 0 & C_{n3} & C_{n1} & -C_{n5} & 0 & -C_{n7} & -C_{n4} \end{bmatrix} \tag{18}$$

At a typical node "i", the constants in $[S]$ are

$$\begin{aligned} C_{i1} &= \frac{y_{i+1} - y_{i-1}}{2} \\ C_{i3} &= \frac{x_{i+1} - x_{i-1}}{2} \\ C_{i4} &= \tfrac{1}{6}[x_i(y_{i+1} - y_{i-1}) + x_{i+1}(2y_{i+1} + y_i) - x_{i-1}(y_i + 2y_{i+1})] \\ C_{i5} &= \tfrac{1}{6}\left[y_i(y_{i+1} - y_{i-1}) + y_{i+1}^2 - y_{i-1}^2\right] \\ C_{i7} &= \tfrac{1}{6}\left[x_i(x_{i+1} - x_{i-1}) + x_{i+1}^2 - x_{i-1}^2\right] \end{aligned} \tag{19}$$

For $n = 3$, a triangular element, C_{i4}, C_{i5}, and C_{i7} are equal to zero. Therefore, for a triangular element, the formulation discussed in this article reduces to a constant stress element.

From Eq. (1), the external work acting on the element can be written as

$$W^{\mathrm{e}} = \{\sigma^*\}^{\mathrm{T}}[S]^{\mathrm{T}}\{a\} \tag{20}$$

The constant strain parameters, ε^*, are determined by equating the internal and external work on the element, Eqs. (10) and (20):

$$\{\varepsilon^*\} = [\lambda]^{-1}[S]^{\mathrm{T}}\{a\} \tag{21}$$

In Eq. (21), the same force–stress matrix, $[S]$, used in Eq. (14) is used to relate strain parameters with nodal displacements. The constant stress parameters, σ^*, are determined using Eq. (4). Next, the left and right sides of Eq. (4) are multiplied by $[H]$ and integrated over the volume of the element:

$$\int_V [H]^{\mathrm{T}}[H]\{\sigma^*\}\,\mathrm{d}V = \int_V [H]^{\mathrm{T}}\{\sigma\}\,\mathrm{d}V \tag{22}$$

Since σ^* is a vector of constants, σ^* can be pulled outside of the integral and solved for

$$\{\sigma^*\} = [\lambda]^{-1}\int_V [H]^{\mathrm{T}}\{\sigma\}\,\mathrm{d}V \tag{23}$$

where σ is related to ε through the particular assumed constitutive relationship. For a linearly elastic material, Eq. (23) simplifies to

$$\{\sigma^*\} = [\lambda]^{-1}\left(\int_V [H]^{\mathrm{T}}[D][H]\,\mathrm{d}V\right)\{\varepsilon^*\} \tag{24}$$

where $[D]$ is the linear elastic material property matrix. The stiffness matrix is determined using Eq. (24) and solving for $\{f\}$ in Eq. (14):

$$\{f\} = [S][\lambda]^{-1}\left(\int_{V^{\mathrm{e}}} [H]^{\mathrm{T}}[D][H]\,\mathrm{d}V\right)[\lambda]^{-1}[S]^{\mathrm{T}}\{a\} \tag{25}$$

Eq. (25) is in the form of $\{f\} = [K]\{a\}$. Therefore, it can be concluded that the element stiffness matrix is

$$[K^{\mathrm{e}}] = [S][\lambda]^{-1}\left(\int_{V^{\mathrm{e}}} [H]^{\mathrm{T}}[D][H]\,\mathrm{d}V\right)[\lambda]^{-1}[S]^{\mathrm{T}} \tag{26}$$

or

$$[K^{\mathrm{e}}] = [S][D^*][S]^{\mathrm{T}} \tag{27}$$

where

$$[D^*] = [\lambda]^{-1}\left(\int_{V^{\mathrm{e}}} [H]^{\mathrm{T}}[D][H]\,\mathrm{d}V\right)[\lambda]^{-1} \tag{28}$$

Since $[\lambda]$ and $[D]$ are symmetric we conclude that $[D^*]$ is also symmetric. Therefore, the element stiffness is also symmetric, as expected. The element stiffness matrix, $[K^e]$, has a rank of seven. Therefore, the formulation is applicable to elements consisting of up to five nodes. For elements having more than five nodes, $[K^e]$ is singular and some type of stabilization parameter is needed to prevent unstable mode shapes. It is important to note that in this formulation a constitutive relationship has not been enforced until Eq. (24); therefore, other than linear material behavior can be easily incorporated.

The element stiffness matrix, Eq. (27), is used to generate the global stiffness matrix through the assemblage step. Nodal displacements are then determined using normal finite element procedures. After nodal displacements are determined, the centroidal strains are calculated from Eq. (21) where the first three elements of the constant strain parameter vector represents centroidal strains. Centroidal stresses are determined from Eq. (24), which can be written as

$$\{\sigma^*\} = [D^*][\lambda]\{\varepsilon^*\} \tag{29}$$

Stresses at any point within the element are determined using Eq. (3).

The previously described formulation assumes a linear stress field. In the early work by Pian, assuming a higher than linear degree polynomial to describe the stress field was not found to significantly influence the element stiffness matrix (Pian, 1964). Although body forces have not been considered in this formulation, body forces can be included with the generalized nodal forces (Tong and Pian, 1969).

As noted by one reviewer of this paper, the element formulation is similar in form to a number of the mixed, or hybrid, formulations noted in the introduction. The key distinguishing feature of the present formulation is the definition of the consistent strain–displacement operator, Eq. (7), combined with the assumption that displacements are linearly varying between nodes at element boundaries, Eqs. (15) and (16). The practical result of these assumptions is that $[\lambda]$ is readily invertible. At this point in the development, it is not clear whether the incompatibility implied by the strain assumption is a serious departure from theoretical requirements for convergence. The performance described in the sections that follow suggests it is not.

An eigenvalue test is applied to the previously discussed formulation to investigate the quality of the linear stress element. Fig. 1 shows eight eigenvalues along with their corresponding shapes for a square four-node linear stress element. Fig. 2 provides similar information for a five-node equilateral element. The original equilateral element in these figures is shown as a dashed line. Both figures show three zero-eigenvalue cases as expected. Each deformed shape corresponding to a zero-eigenvalue represents an independent rigid-body motion. The rigid-body motions in these figures show a combined translation and rotation deformation. Besides the rigid body motion, no additional zero-energy modes are indicated. For the four-sided element, eigenvectors four and five have the same eigenvalues and are comparable to within a rotation. Eigenvector six for the square represents a pinching mode, while seven is pure shear. Lastly, eigenvector eight is an isotropic extension. For the five-node element, eigenvalues four and five, six and seven, and eight and nine are equal. These eigenvectors represent a combination of extension, bending, and shear modes. Eigenvalue ten corresponds to isotropic extension.

In the following sections, the suitability of the linear stress formulation described in this article is investigated through patch tests and example problems.

3. Examples

3.1. Patch tests

Two patch tests are conducted to validate the proposed formulation by investigating a mesh comprised of elements of four and five nodes. A linear stress distribution is assumed within each element. The nodal

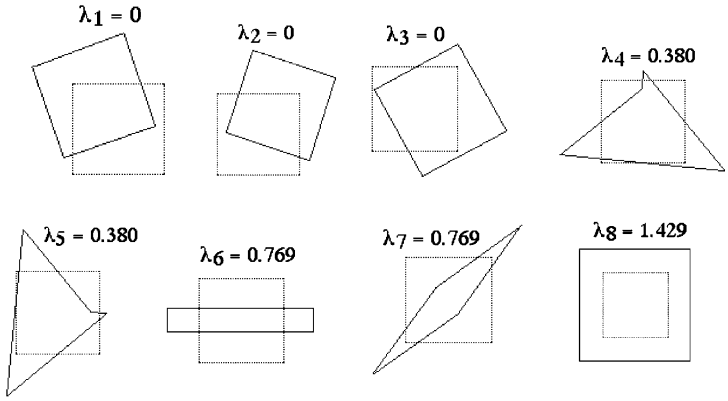

Fig. 1. Eigenvalues and eigenvalue shapes for a square linear stress element ($E = 1$; $v = 0.3$).

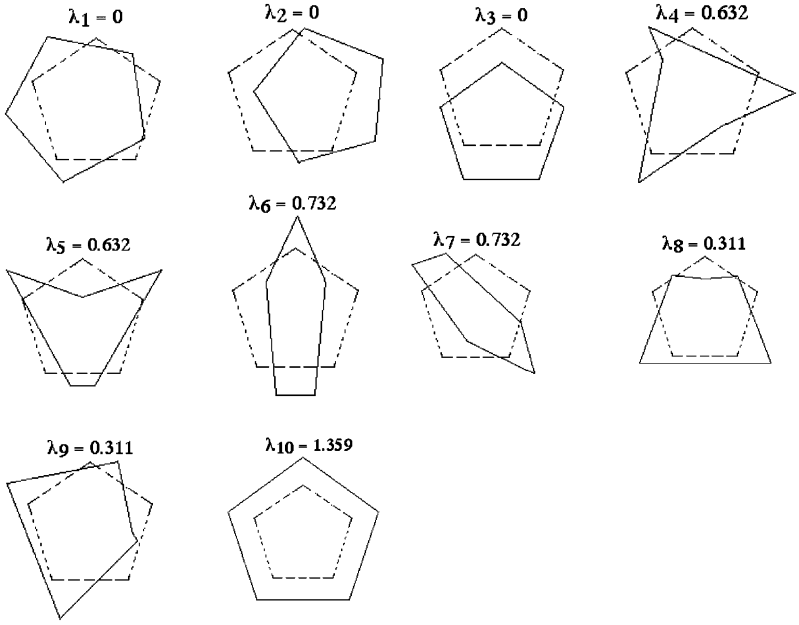

Fig. 2. Eigenvalues and eigenvalue shapes for a five noded equilateral polygon ($E = 1$; $v = 0.3$).

loads in these tests represent a uniformly distributed stress condition along the element boundary and are applied to the mesh to create a constant stress condition for σ_{xx}, σ_{yy}, and τ_{xy}. The computed stresses from the numerical solution are then compared with the analytic solution. The finite element mesh used for this analysis is similar to the one included in the reference by Cook et al. (1989), however considers elements comprised of more than four nodes. Boundary conditions are set to prevent rigid body movement. The patch tests considered use a plane strain problem in which Young's Modulus, E, is equal to 20.68 MPa (3000 psi), and a Poisson's ratio, v, of 0.3.

The constant σ_{xx} patch test is shown in Fig. 3. The figure shows the mesh with the applied loading to produce a theoretical constant σ_{xx} stress distribution throughout the patch. In the test, F equals 444.8 N (100 lb). The figure illustrates the deformed shape. Results show constant σ_{xx} stress throughout the mesh

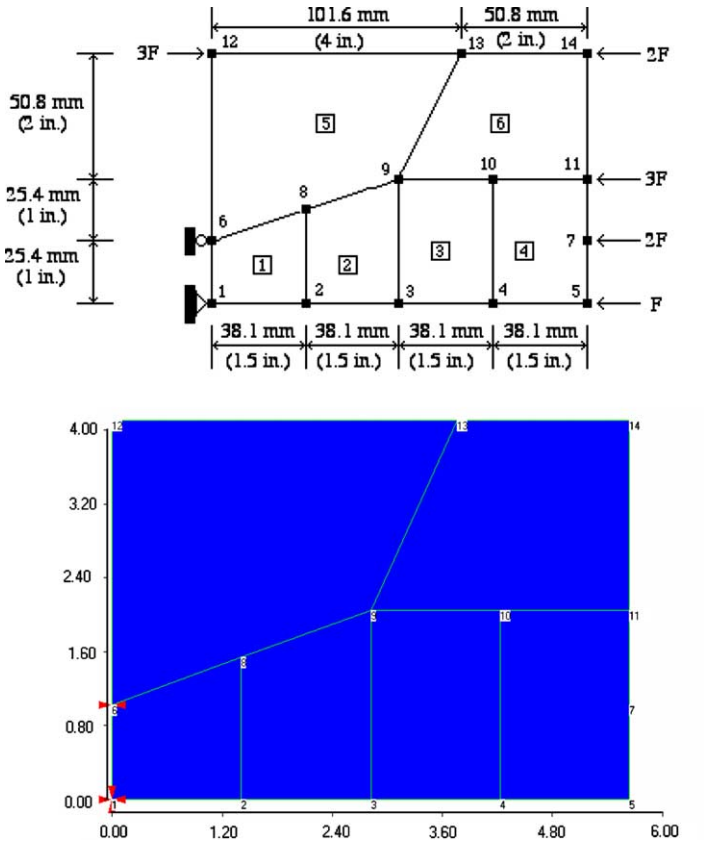

Fig. 3. Horizontal stress patch test.

and the numerical solution matches well the analytic solution. The numeric results for stress are within 2.34E−12 kPa (3.39E−13 psi) of the analytic solution of $\sigma_x = 1379.0$ kPa (200.0 psi), and $\sigma_y = \tau_{xy} = 0$. End displacements at node 14 are within 6.96E−09 mm (2.74E−10 in.) of the analytic solution $u = -9.246$ mm (−0.3640 in.) and $v = 2.642$ mm (0.1040 in.).

The second patch test examines the case of an applied uniformly distributed shear stress, Fig. 4. The uniformly distributed shear stress is represented through nodal loads with F equal to 44.48 N (10 lb). The boundary conditions for this test are the same as the σ_{xx} patch test case in Fig. 3. The deformed shape for the second patch test is shown in Fig. 4. Numerical results show a constant shear stress, τ_{xy}, distribution throughout the patch test mesh. Stresses are within 1.0977E−12 kPa (1.592E−13 psi) of the analytic solutions, $\tau_{xy} = 137.90$ kPa (20 psi), $\sigma_{xx} = 0$ kPa, and $\sigma_{yy} = 0$ kPa. Numeric end displacements are within 8.805E−09 mm (3.4666E−10 in.) of the analytic solutions $u = 0.0$ mm and $v = -2.642$ mm (−0.1040 in.).

The previous patch tests substantiate the proposed formulation of the linear stress element described in this paper. In the following section, a cantilever beam example is used to examine the convergence of the linear stress element.

3.2. Cantilever beam example

A cantilever beam is examined as a plane strain problem to determine the suitability of the linear stress element formulation and its rate of convergence. Results from a mesh consisting of rectangular elements are

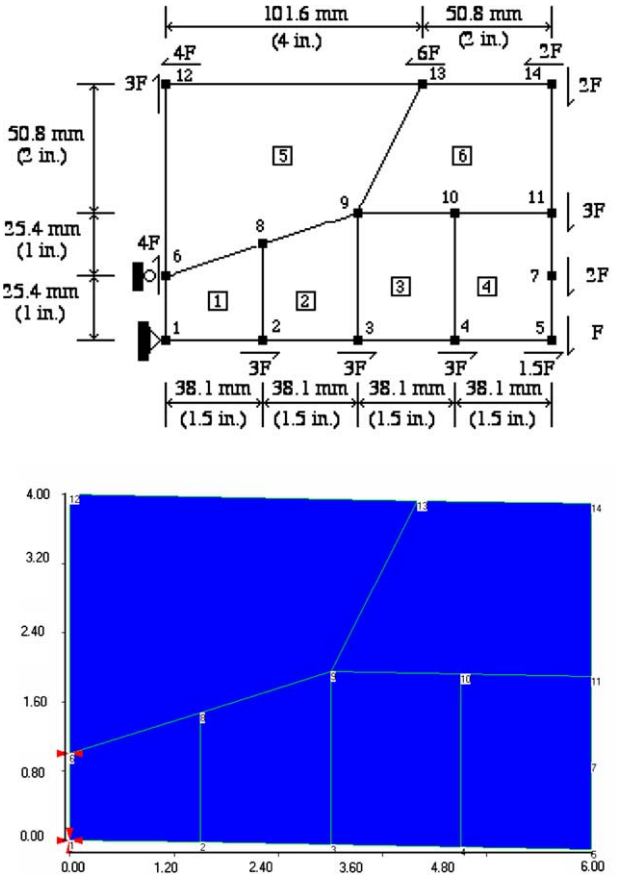

Fig. 4. Shear stress patch test.

compared with a mesh using triangular elements, Fig. 5. Fig. 5 shows the cantilever beam discretized using 16 equal rectangular elements. However, four mesh configurations are considered using 16, 64, 256, and 1024 rectangular elements. Mesh configurations beyond the 16-element case are established by subdividing each of the elements equally in the horizontal and vertical directions. A 17-element triangular element mesh is shown in Fig. 5. Four triangular meshes are investigated using 17, 66, 260, and 1032 elements. The triangular element mesh is refined by creating new element boundaries, which join previous element boundary midpoints. Two load cases are examined for convergence, a cantilever beam subjected to an end moment of 13.49 kN mm, case M(1), and a cantilever beam subjected to an end shear force of 0.10 kN, case V(2) and case V(3) using rectangular and triangular elements respectively. Values were selected for the plane strain problem to develop the same analytic end displacement of 4.00 mm for the two applied force cases. An elastic modulus, E, of 70.0 GPa and a Poisson's ratio, v, of 0.35 are used. Two additional Poisson's ratios 0.45 and 0.49 are also considered to examine the behavior of the element as the material tends toward becoming incompressible. Results for the three cases, M(1), V(2), and V(3), are given in Fig. 6 as a convergence plot of displacement error and normalized element height. Lines in the figure are identified according the particular case and Poisson's ratio.

In the first case using $v = 0.35$, convergence is examined for an applied end moment, M(1). Concentrated loads are applied along the end node points to develop a 13.49 kN mm end moment. Although the

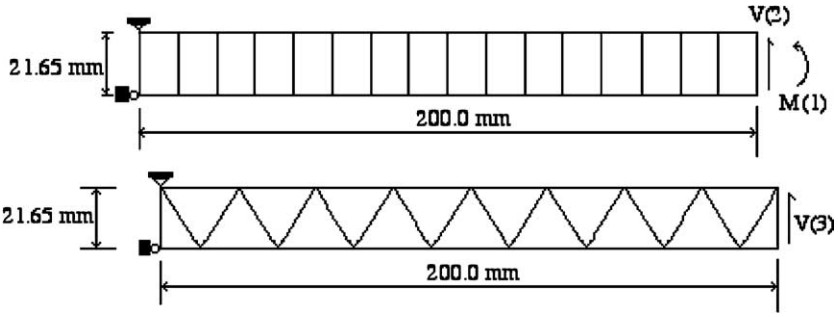

Fig. 5. Mesh configurations used to evaluate a cantilever beam with end loads.

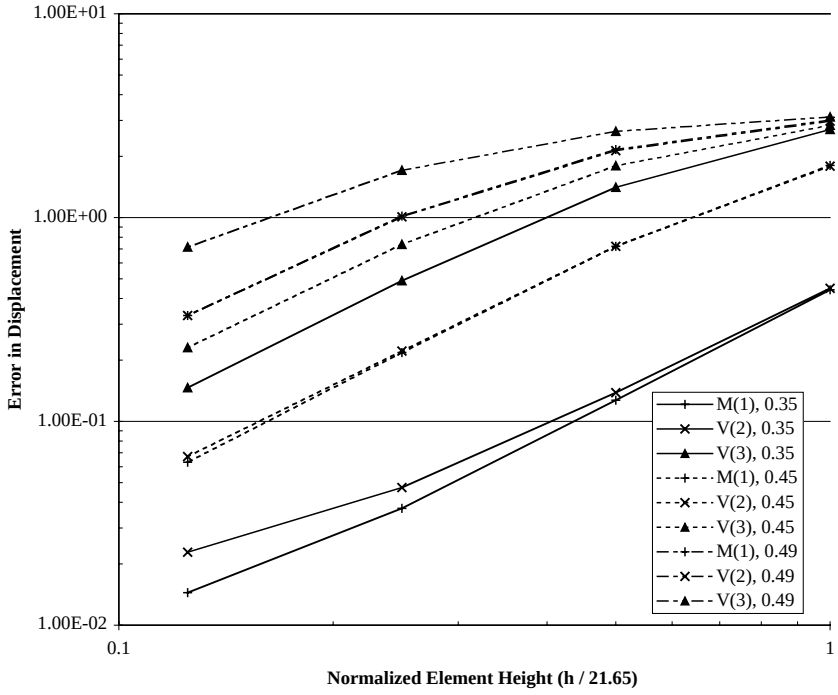

Fig. 6. Cantilever beam convergence plot.

numerical solution for 16 rectangular elements (3.558 mm) does not match the analytic solution (4.000 mm), the error is small even for this coarse mesh, and convergence to the analytic solution is quick.

In the second and third cases using $v = 0.35$, the beam is analyzed for an end shear and is examined using rectangular elements, V(2), and triangular elements, V(3). Consistent loads at node points are used to represent the uniformly distributed shear force at the free end. Results from meshes comprised of triangular elements are included to compare convergence between element types for this particular load case. The calculated end displacements along the member centroidal axis for each of these discretization schemes is compared with the analytic solution, 4.00 mm. In the linear stress formulation discussed in this article, a triangular element of three nodes reverts to a constant stress element. Therefore, convergence to the

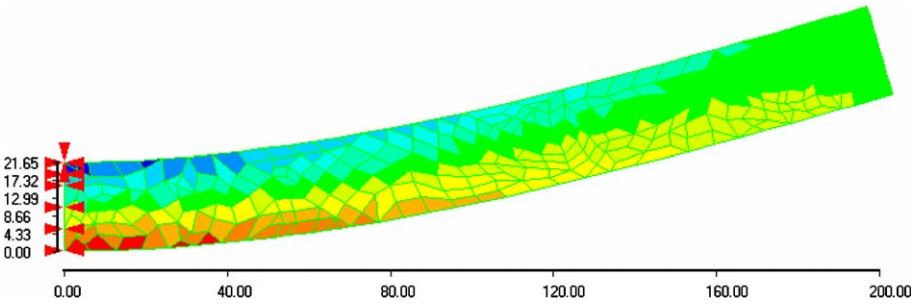

Fig. 7. Cantilever beam response using a random mesh distribution.

analytic solution using the triangular element is slow and requires a highly discretized domain to attain reasonable results.

Results for the cantilever problem are also given for the three cases using $v = 0.45$ and 0.49. Fig. 6 shows that for this element formulation, as the material Poisson's ratio increases the error in the end displacement increases; however, the rates of convergence do not differ significantly. A stress element consisting of five stress parameters was examined to determine if reducing the number of stress parameters would improve the behavior of the element at higher Poisson's ratios. The end displacements for a Poisson's ratio of 0.49 were computed with a larger error than the seven stress parameter element, although the convergence rates of the two were similar.

To illustrate the robustness of the linear stress formulation, the same cantilever beam using $v = 0.35$ and an end shear, 0.10 kN, is examined using an arbitrarily developed mesh distribution consisting of 384 elements, Fig. 7. Quadrilateral elements are primarily used, however a few triangular elements are required. The deformed shape of this beam due to the end shear is shown in Fig. 7. The gray shades within the beam represent σ_{xx} stress contours. The calculated free-end displacement at the member centroidal axis is 3.832 mm. This result shows good agreement with the analytic solution, 4.00 mm, even for this case using an unsymmetrical mesh distribution comprised of randomly generated elements.

3.3. Comparison with the constant strain rectangular element

To compare the benefits of the linear stress element formulation over the constant strain formulation, the same cantilever beam problem with an end shear of 0.10 kN using 256 rectangular elements and $v = 0.35$ is solved using the constant strain element. Fig. 8 shows the singularity that occurs when the stabilization problem inherent to the constant strain element formulation is not addressed. The displacement scale has been greatly reduced for presentation. The "hourglassing" which occurs in the constant strain element is remedied by using a stabilization parameter to constrain 'hourglassing' (Peters and Heymsfield, 2003). Fig. 9 shows the response of the cantilever beam using a small stabilization factor. Note

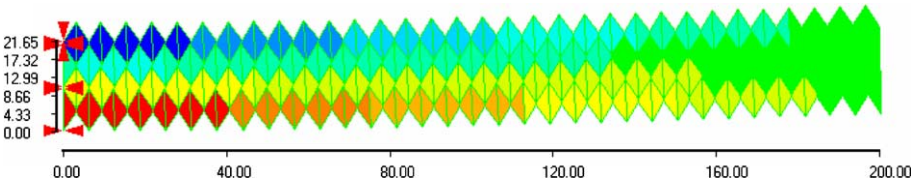

Fig. 8. Cantilever beam response using constant strain elements without stabilization.

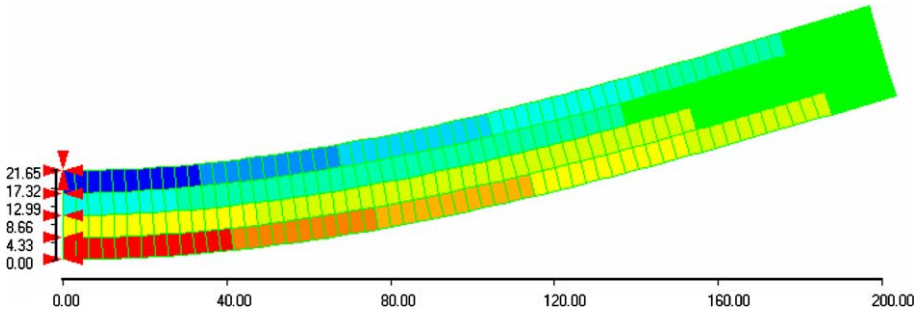

Fig. 9. Cantilever beam response using constant strain elements with stabilization.

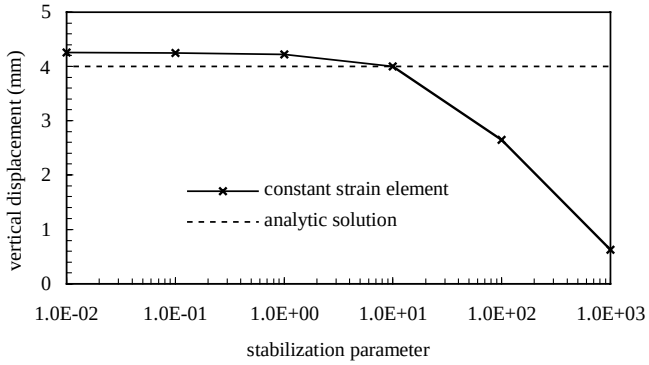

Fig. 10. Cantilever beam end displacement considering constant strain elements.

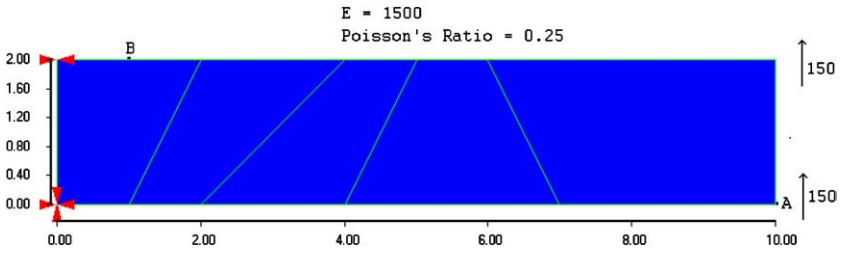

Fig. 11. Five element cantilever beam with end shear loading.

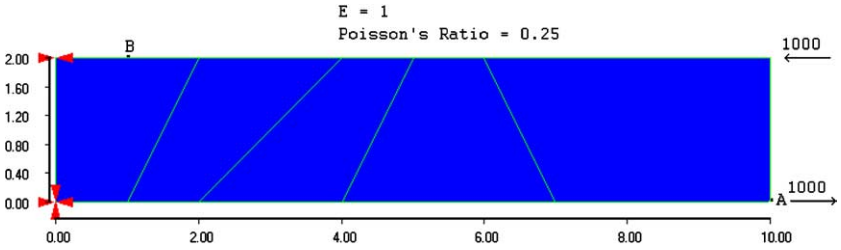

Fig. 12. Five element cantilever beam with end moment.

Table 1
Comparison of plane stress solutions for a five-element cantilever beam subjected to an end shear force

Element	v (A)	σ_x (B)
Q4	50.96	−2448
QM6	97.98	−3453
P-S	98.05	−3899
QE2	98.26	−3906
Present method	69.08	−3453
Exact	102.6	−4050

Table 2
Comparison of plane stress solutions for a five-element cantilever beam subjected to an end moment

Element	v (A)	σ_x (B)
Q4	45.65	−1604
QM6	96.07	−2497
P-S	96.18	−3001
QE2	96.5	−3004
Present method	69.08	−2521
Exact	100	−3000

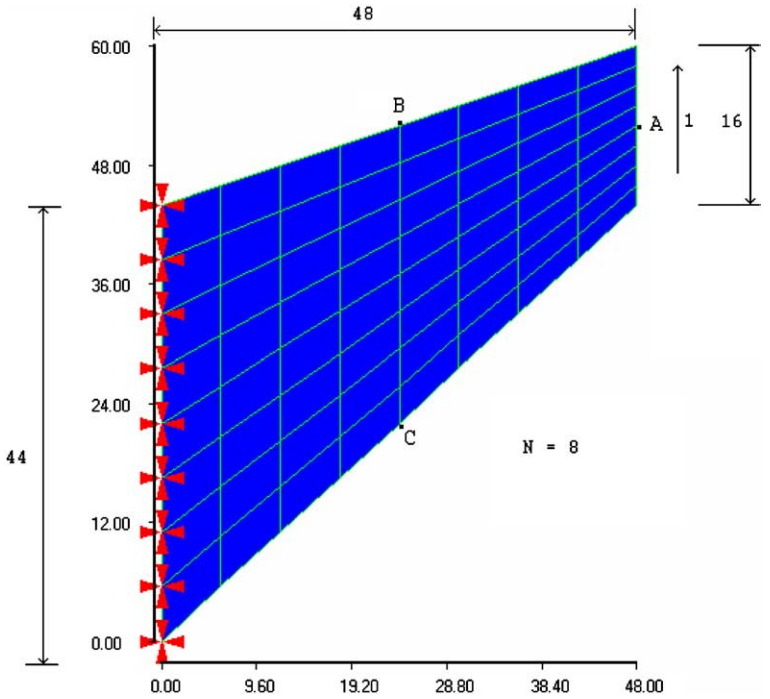

Fig. 13. Cook's membrane problem ($E = 1$, $v = 1/3$).

that "hourglassing" is still present and that the end displacement for this case is overestimated, 4.258 mm, as compared to the analytic solution, 4.00 mm.

To illustrate the significance of the stabilization parameter value, a plot showing the end displacement as a function of the stabilization parameter used for this problem is presented in Fig. 10. The figure shows the convergence of the constant strain element to the exact solution as a function of the stabilization parameter value. Fig. 10 also shows the problem in selecting the stabilization parameter solely as an arbitrarily large number. The convergence trend as a function of stabilization parameter overestimates the solution and shows little variance up until $s = 10$; however, beyond this value, the end displacement dramatically decreases. Fig. 10 shows that using an arbitrarily large number for the stabilization parameter can lead to over stiff behavior.

In the following sections, additional problems are tried to examine the suitability of the linear stress element formulated in this article.

3.4. Element distortion

Element distortion is investigated in Figs. 11 and 12. Fig. 11 is a five element cantilever beam with an end shear. Fig. 12 is the same cantilever beam mesh with an end moment using two axial node forces. Results for the end shear loading problem are given in Table 1 and for the end moment problem in Table 2. Tables 1 and 2 also include results from other element formulations which are taken from Piltner and Taylor (1995). These elements include the bilinear isoparametric displacement element (Q4); the enhanced strain element by Taylor, Beresford, and Wilson (QM6); Pian and Sumihara's hybrid stress element; and the enhanced mixed element QE2 by Piltner and Taylor. The stress at point "B" for the present method is

Table 3
Comparison of plane stress solutions for Cook's membrane problem using $N = 16$

Element	v (A)	σ_{min} (B)	σ_{max} (C)
Q4	23.43	−0.1995	0.2353
QM6	23.88	−0.2025	0.2364
P-S	23.88	−0.2025	0.2364
QE2	23.88	−0.2025	0.2364
Present method	23.65	−0.1975	0.2310

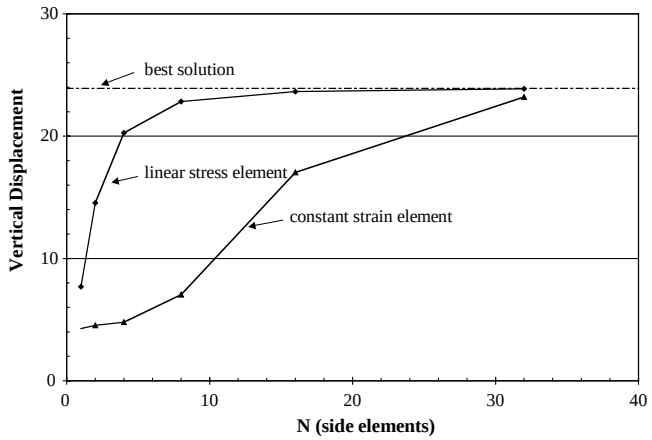

Fig. 14. End displacement for Cook's membrane problem as a function of number of elements.

determined using Eq. (3) while the other element formulations calculate the stress as an average of the adjacent node values. The present method shows superior behavior over the bilinear isoparametric element, but is outperformed by the other more sophisticated elements. However, a consideration in comparing these elements is the CPU time. Solution of the linear stress element presented in this article is based on using a single point to describe the stress variation within the element and therefore uses minimal computation time.

3.5. Cook's membrane problem

Cook's membrane problem is investigated to examine the performance of the element in a skewed mesh (Cook, 1987). The problem is illustrated in Fig. 13. The figure shows a tapered cantilever beam subjected to an end shear force. The shear force is uniformly distributed over the beam end. The left support is rigid and modeled by preventing translation in either direction at each boundary node point. The figure shows the case of using eight side elements and therefore a total of sixty-four elements. Results for the displacement at "A", and stresses at "B" and "C" are provided in Table 3. The table also includes similar results for the same element formulations discussed in the previous mesh distortion section. The stresses at these points for

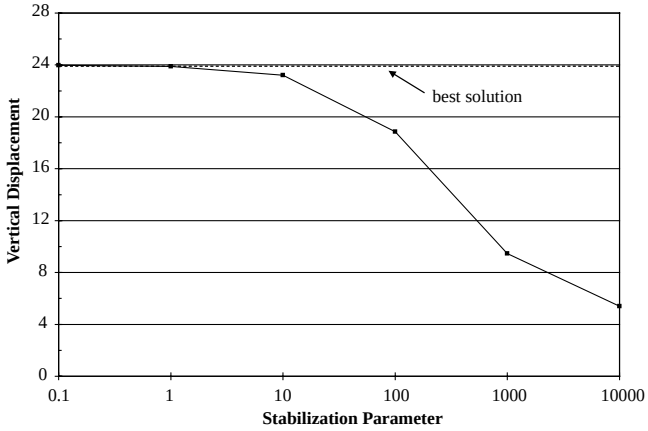

Fig. 15. Cook's membrane problem, end displacement as a function of stabilization parameter using constant strain elements.

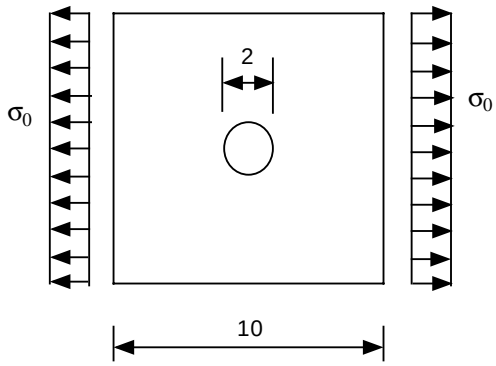

Fig. 16. Tension strip with a small circular hole.

the present method are determined using Eq. (3) for each adjacent element and averaging these values. Fig. 14 is a convergence plot for the problem showing the quick convergence of the linear stress element. Results using the constant strain element are also superimposed on the figure. Again to illustrate the dependency of end displacement to the stabilization parameter in a constant strain element, Cook's membrane problem is solved using 32 side elements, $N = 32$. For this particular problem, the end displacement solution is highly dependent on the value chosen for the stabilization parameter as shown in Fig. 15.

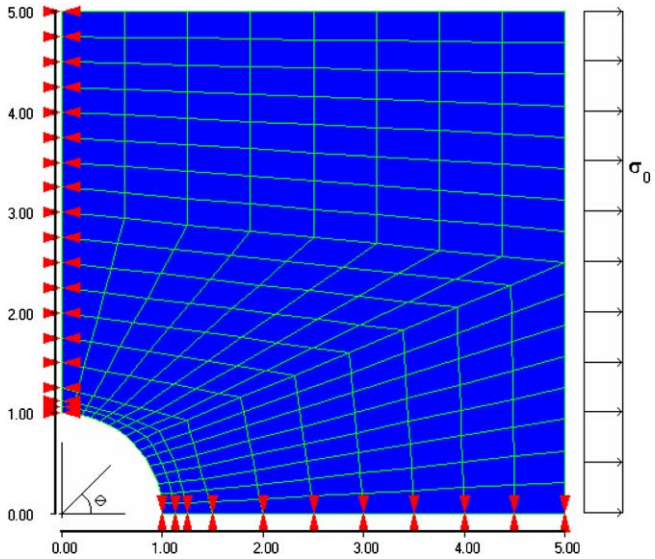

Fig. 17. Finite element mesh for tension strip problem.

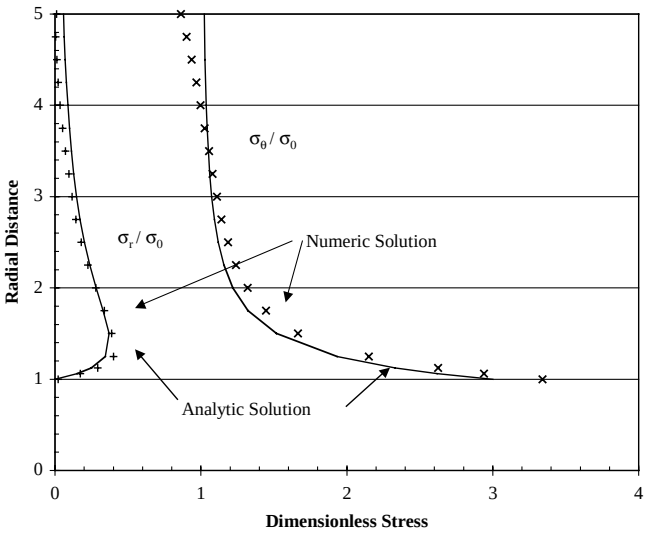

Fig. 18. Stress results at $\theta = \pi/2$ for a tension strip with a small concentric hole.

3.6. Tension strip problem

The last problem investigated is a tension strip with a small concentric circular hole. The problem is shown in Fig. 16. The problem is symmetric and therefore modeled using a quarter of the plate, Fig. 17. Stress results are given along the vertical axis of symmetry and shown in Fig. 18. Stresses are determined using Eq. (3) and averaged for adjacent elements. Analytic results assuming a large plate and a small circular hole are superimposed on Fig. 18 (Ugural and Fenster, 2003). The results show good agreement for the selected mesh.

4. Conclusions

A linear stress element has been formulated that is applicable to polygonal elements of up to five nodes. For a three noded element, triangle, the formulation simplifies to a constant stress element. Although the formulation has been developed assuming a linear elastic material, the work can be extended to apply to nonlinear materials. The element has been formulated through virtual work and by equating the internal work of the element stresses with the external work of surface tractions on the element boundary. The adequacy of the formulation and code implementation of the linear stress element has been investigated by examining the element's robustness through sample problems and patch tests. Good results for these problems have confirmed the linear stress formulation discussed in this article. Two problems, a cantilever beam with a tip load and Cook's membrane problem, were solved using the constant strain element. Results from the constant strain element show the dependency of displacement on the stabilization parameter value and therefore, the weakness of the constant strain element as compared to the linear stress element. Solution of the linear stress element presented in this paper is based on parameters at the element's centroid. Therefore, CPU time is comparable with the constant stress element. In this manuscript, the linear stress element has been developed for a two-dimensional problem; however, extension of this work to a three-dimensional problem is straightforward.

Acknowledgements

This paper was prepared from research conducted under the Geotechnical Engineering Research Program and Earthquake Engineering Research Program of the Engineer Research and Development Center, Waterways Experiment Station, Vicksburg, MS. Permission was granted by the Chief of Engineers to publish this information.

References

Cook, R.D., 1987. A plane hybrid element with rotational D.O.F. and adjustable stiffness. International Journal for Numerical methods in Engineering 24, 1499–1508.

Cook, R.D., Malkus, D.S., Plesha, M.E., 1989. Concepts and Applications of Finite Element Analysis. John Wiley, New York.

Gallagher, R.H., 1965. Comments on derivation of element stiffness matrices by assumed stress distributions. AIAA Journal 3 (1), 186–187.

Peters, J., Heymsfield, E., 2003. Application of the 2-D constant strain assumption to FEM elements consisting of an arbitrary number of nodes. International Journal of Solids and Structures 40 (1), 143–159.

Pian, T.H.H., 1964. Derivation of element stiffness matrices by assumed stress distributions. AIAA Journal 2 (7), 1333–1336.

Pian, T.H.H., 2000. Some notes on the early history of hybrid stress finite element method. International Journal for Numerical Methods in Engineering 47, 419–425.

Pian, T.H.H., Sumihara, K., 1984. Rational approach for assumed stress finite element. International Journal for Numerical Methods in Engineering 20, 1685–1695.

Piltner, R., Taylor, R.L., 1995. A quadrilateral mixed finite element with two enhanced strain modes. International Journal for Numerical Methods in Engineering 38, 1783–1808.

Piltner, R., Taylor, R.L., 1999. A systematic construction of B-bar functions for linear and non-linear mixed-enhanced finite elements for plane elasticity problems. International Journal for Numerical Methods in Engineering 44, 615–639.

Simo, J.C., Armero, P., 1992. Geometrically non-linear enhanced strain mixed methods and the method of incompatible modes. International Journal for Numerical Methods in Engineering 33, 1413–1449.

Simo, J.C., Rifai, M.S., 1990. A class of mixed assumed strain methods and the method of incompatible modes. International Journal for Numerical Methods in Engineering 29, 1595–1638.

Tong, P., Pian, T.H.H., 1969. A variational principle and the convergence of a finite-element method based on assumed stress distribution. International Journal of Solids and Structures 5, 463–472.

Ugural, A.C., Fenster, S.K., 2003. Advanced Strength and Applied Elasticity, fourth edition. Prentice-Hall, Upper Saddle River, NJ.

Wolf, J.P., 1975. Alternate hybrid stress finite element models. International Journal for Numerical Methods in Engineering 9, 601–615.